

Distribution of cold and temperate ice and water in glaciers at Nordenskiöld Land, Svalbard, according to data on ground-based radio-echo sounding



Yuri Macheret* ^a, Andrey Glazovsky ^b, Ivan Lavrentiev ^c

Russian Academy of Sciences, Russia

* Correspondence: Russian Academy of Sciences, Russia. E-mail: macheret2011@yandex.ru

^a <https://orcid.org/0000-0001-5687-5381>, ^b <https://orcid.org/0000-0001-6275-7517>, ^c <https://orcid.org/0000-0002-6902-7186>

Abstract. The distribution of cold and temperate ice and water in polythermal glaciers is an important characteristic in studying their thermal regime, hydrology, and response to climate change. Data analysis of ground-based radio-echo sounding of 16 glaciers in Nordenskiöld Land in Spitsbergen shows that 5 of them are of cold type and 12 are of polythermal type. The mean thickness of cold and temperate ice in polythermal glaciers varies from 11 ± 2 to 66 ± 6 m and from 6 ± 2 to 96 ± 9 m, respectively, and their ratio varies from 0.30 to 5.31. The volume of temperate ice in polythermal glaciers varies from 0.0009 to $3.733 (\pm 10\%) \text{ km}^3$. With water content of 2% in temperate ice in these glaciers they might contain in total up to $\sim 93.5 \times 10^6 \text{ m}^3$ of liquid water. Radar data suggest the greater water content or greater size of water inclusions in near-bottom temperate ice.

Key words:
 Nordenskiöld Land,
 polythermal glacier,
 radio-echo sounding,
 Svalbard

Introduction

Polythermal glaciers, which contain both cold ice (i.e. below the pressure melting point) and temperate ice (i.e. at the pressure melting point), are widely distributed in Svalbard.

The presence of liquid water remarkably influences the deformation rate of glacier ice (Duval 1987). Therefore, it is important to know the distribution of cold and temperate ice masses in glaciers and ice sheets in order to model their dynamics and bottom conditions and estimate their responses to climate change (Blatter and Greve 2015; Hewitt and Schoof 2017; Glazovsky and Macheret 2014). This is particularly important for modern glaciation in Svalbard, Norway – with 1,567 glaciers and a total ice-covered area of $\sim 33,837.5 \text{ km}^2$ (Pfeffer et al. 2014; RGI Consortium 2017) – where 345 gla-

ciers were attributed to the surge type (Sevestre et al. 2015). Switches between cold- and warm-based conditions have long been invoked to explain surges (i.e. flow instability) in polythermal glaciers in Svalbard (Murray and Porter 2001).

The distribution of temperature and water in glacier bodies depends on many factors (Aschwanden and Blatter 2005; Aschwanden et al. 2012) since the heat sources are on a glacier's surface, at bedrock, and within a glacier. External heat enters a glacier by means of conduction resulting from the advection of moving ice and water, as well as air convection through crevasses, conduits and moulins. Internal heat sources include dissipative warming (internal friction), ice deformation, ice friction at bedrock, the friction of flowing water in englacial channels, repeated freezing of water, ice melting and geothermal flux. These factors are the main determinants of the distribution of cold and temperate

ice and water in glacier sequences and at the bedrock of glaciers.

The qualitative remote sensing indicator of polythermal glaciers is the extended internal reflecting horizon (IRH) at cold-temperate surface (CTS), an interface between cold and temperate water-containing ice registered by the data of radio-echo sounding (RES) (Macheret and Zhuravlev 1982; Bamber 1987, 1988, 1989; Dowdeswell et al. 1984). The correctness of such an interpretation confirms a close (to within several metres) coincidence of depths of CTS by data RES measurements and ice temperature measurements in boreholes on Fridtjovbreen and other Svalbard glaciers of the polythermal type (Björnsson et al. 1996; Ødegaard et al. 1997; Macheret and Glazovsky 2000).

The quantitative remote sensing indicator of polythermal glaciers is that the radio wave velocity (RWV) is lower in temperate ice compared to cold ice (Macheret and Glazovsky 2000; Barrett et al. 2007). The wide distribution of polythermal glaciers in Svalbard was shown by airborne RES measurements performed from 1970 to the 1980s, which detected anywhere from 50 (Jiscot et al. 2000) to 85 (Glazovsky et al. 1988) glaciers with IRH. Later ground-based RES studies of hydrothermal structure were carried out at a number of Svalbard polythermal glaciers (Björnsson et al. 1996; Jania et al. 2005; Navarro et al. 2005, 2016; Bælum and Benn 2011; Martin-Español et al. 2013; Glazovsky and Macheret 2014; Sevestre et al. 2015). Changes in the hydrothermal structure of two glaciers in Nordenskiöld Land (NL) were discussed by Vasilenko et al. (2014).

In this paper, we consider the distribution of cold and temperate ice and water in 16 glaciers in NL using data from ground-based measurements at a frequency of 20 MHz obtained in 1999, 2007, and 2010–2013 (Fig. 1) before spring melting starts. Most of the studied glaciers are land-terminating, with areas of more than 0.5 km² and lengths from 2 to 11.5 km. Only one of the largest glaciers, Fridtjovbreen, is 13 km long and 47.1 km² in area, terminates in the sea, and is of the surge type. Its last surge was observed in the 1990s and lasted seven years, accompanied by the formation of a great number of crevasses (Murray et al. 2012).

In previous publication (Lavrentiev et al. 2019) these data were used to estimate the total ice vol-

umes of these glaciers and in the total in NL. In this paper we present new data on the thickness and volume of cold and temperate ice and the distribution of water in glacier sequence, at glacier bottom, and CTS.

Methods

Radar equipment

For RES measurements we used the monopulse ground penetrating radars (GPR) VIRL-6 (Macheret et al. 2006) and VIRL-7 (Vasilenko et al. 2011) with a central frequency of 20 MHz, pulse duration of 25 ns, and sampling interval of 2.5 ns, supplied with a digital recording system (control unit) for registration of the radar signals and global positioning system (GPS) data with an interval of 0.2 s (~1 m) and accuracy of georeferencing ± 5 m. The antennas consist of four flexible, lightweight, resistively loaded dipoles with central frequency of 20 MHz. Each dipole has a length of 5.8 m and consists of 18 resistors and 20 metal wires, all of them cored by a polypropylene cable, allowing us to tie the antennas to a sledge or slings.

Measurements

Ground-based ice thickness measurements (profiling) were carried out automatically at a frequency of 0.2–0.4 s. Radar components (transmitter, receiver, control unit, batteries, antennas and GPS) were mounted on two specially constructed wooden sledges (in 1999, 2011, 2012 and 2013) and on two plastic pulkas (in 2007, 2010 and 2012), which were towed over glacier surfaces by a snowmobile at a speed of 10–20 km hr⁻¹. A conventional GPS (Garmin GPSMap 76x) was used to record plane coordinates every 2 sec. Radar signals were transmitted and received using the 5.8-m-long resistively loaded dipole antennas with a distance between their centres of 10 m. To synchronise the signals from antennas, a fibre-optic cable was used. The mean distance between measurement points varies from 0.2 m to 15 m. The total length of radar pro-

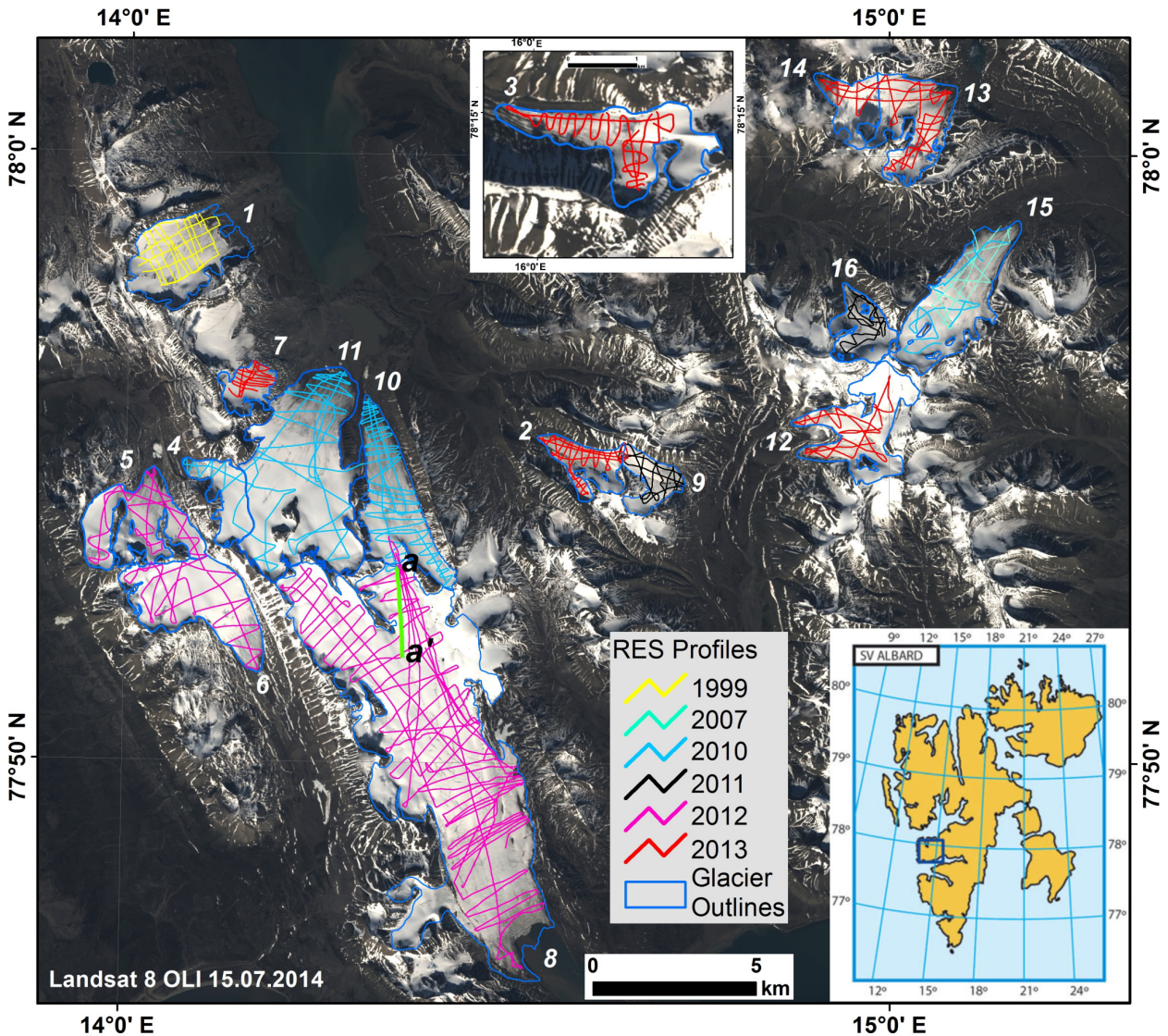


Fig. 1. Profiles of ground-based RES measurements in springs 1999, 2007 and 2010–2013 in Nordenskiöld Land on glaciers: 1 – Aldegondabreen, 2 – Baalsrudbreen, 3 – Blekumbreen, 4 – Austre Dahlfonna, 5 – Vestre Dahlfonna, 6 – Erdmannbreen, 7 – Vestre Field (formerly part of Vestre Grønfyordbreen), 8 – Fridtjovbreen, 9 – Gleditschfonna, 10 – Austre Grønfyordbreen, 11 – Vestre Grønfyordbreen, 12 – Marstranderbreen, 13 – Austre Passfjellbreen, 14 – Vestre Passfjellbreen, 15 – Tavleebreen, 16 – Tungebreen; colour lines show the location of RES profiles, and blue outlines show the glacier boundaries for the year of RES measurements; thick black line (a–a’) indicates the section of profile 439_15 that corresponds to the location of the radargram in Figure 2; in the inset, a small square shows the location of the study area

files was ~600 km: (see Fig. 1) where ~31 km was made on Aldegondabreen, 22 km on Baalsrudbreen, 14 km on Blekumbreen, 9 km on Austre Dahlfonna, 26 km on Vestre Dahlfonna, 31 km on Erdmannbreen, 173 km on Fridtjovbreen, 19.5 km on Gleditschfonna, 53 km on Austre Grønfyordbreen, 102 km on Vestre Grønfyordbreen, 15 km on Vestre Field, 25 km on Marstranderbreen, 35 km on both

Passfjellbreen, 33 km on Tavleebreen and 12.5 km on Tungebreen.

Data processing

For visualisation and further processing of RES and GPR data, we used the software RadExPro (www.radexpro.ru, Kulnitsky et al. 2000). Standard pro-

cedures were applied to the raw radar data for amplitude correction, bandpass filtering, 2-D spatial filtering and Stolt-FK migration (to obtain the real geometry of the bedrock by correcting the position of the lateral reflections using Fourier analysis). Picking was used for manual digitising of the time delay of reflected signals in interactive mode. Also, the SSAA module was applied to measure the relative power of reflections and the Diffraction module served for estimation of RWV in cold and temperate ice using hyperbolic reflections of symmetric form from CTS, crevasses and bedrock.

Several types of reflected signals were detected on the obtained radargrams. The first type was the reflected signals from the surface and intraglacial inhomogeneities (e.g. crevasses and water impurities in temperate ice). They were a source of strong scattering of radio signals in ice saturated with melt water (which is typical of temperate ice). Reflections of the second type were from the ice/subglacial bed interface (see Fig. 2). These reflections were represented by hyperbolas from individual point reflectors at the basal layers, or continuous lines along the measurement profiles.

After data processing, a summary table of UTM-coordinates (x , y) and the delay time (τ) of the digitised bedrock was compiled, and the glacier thickness was calculated using an average speed of 0.168 m/ns for radio-wave propagation in the glacier (Dowdeswell and Evans 2004). In the final step, ice-thickness point data, together with data on zero thickness at glacier margins, were used to construct the ice thickness maps.

Results of radar measurements

Subsurface reflections in polythermal glaciers

As already mentioned, an important remote sensing indicator of polythermal glaciers is IRH on radar records.

Additional information on the internal structure of glaciers is provided by the vertical series of hyperbolic reflections (VSHR) from buried crevasses and/or glacier moulines, which indicate the possible sites, depths and pathways of melt water

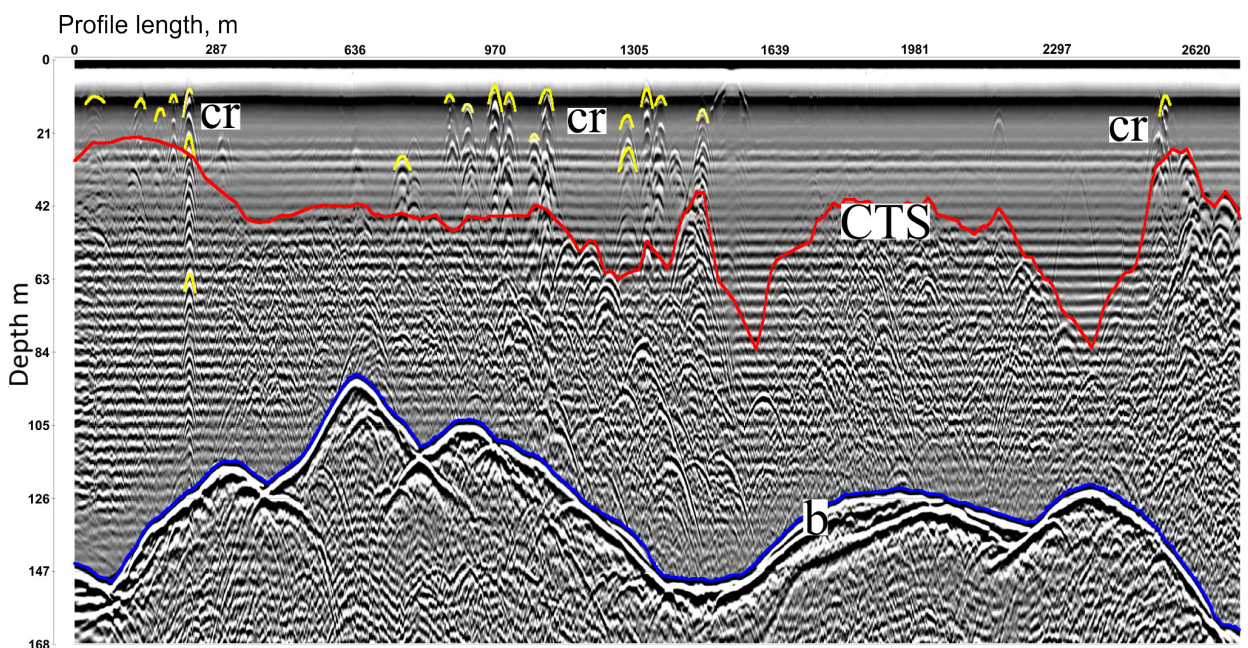


Fig. 2. An example of a radargram 439_15 obtained on Fridtjovbreen. Vertical and horizontal scales indicate the ice depth (estimated with radio wave velocity 168 m/mcs) and distance along the route. Reflections from CTS, near-surface crevasses (cr) and bedrock (b) are shown in red, yellow, and blue, respectively. The location of the section is shown in green (a-a') in Figure 1

entering into glaciers during melting periods and penetrating to near-bottom temperate ice layers and bedrock. Typical examples of radar records with reflections from CTS and buried crevasses and/or glacier moulines are shown in Figure 2.

Relative power of subsurface reflections

According to the theory of Mie (Bamber 1988), the power (intensity) of scattering radio waves on air and water inclusions in ice depends on their size and the radar frequency. At a frequency of 20 MHz, the maximal scattering on water inclusions in temperate ice takes place at their radius of 0.25–0.4 m and by 20–30 dB, which is more than on air inclusions of the same size. Therefore, the difference in scattering values on such inclusions can be used to more reliably estimate the origin of reflections of different types in radar records. This aim can be achieved using data of measurements with impulse radars of the power reflection coefficient (PRC) of reflections from CTS and bedrock (Bamber 1987, 1989).

In our case, we used the monopulse radar records and the SSAA module to measure the uncalibrated root mean square (rms) amplitudes A_t and A_r of transmitted and reflected signals within a time window of 80 ns exceeding 2–3 times the duration of the transmitted pulse. As a result, we calculated the relative power of reflections (RPR) from subsurface reflectors including bedrock, buried crevasses, moulines and water inclusions in temperate ice beneath CTS. To take into account the dependence of RPR on depth h of reflectors, we used the simplified radar equation adapted for ground-based RES measurements with antennas on glacier surfaces and calculated the RPR of reflected signals as:

$$RPR = 20 \lg (A_t / A_r) - 20 \lg (h / \epsilon_i^{1/2}) - 2zB, \quad (1)$$

where $h = v_{av} \tau / 2$ and $v_{av} = 168$ m/mcs is the average RWV in the glacier, τ is the delay time of reflected signals, $\epsilon_i = 3.19$ is the relative dielectric permittivity of ice, and $B = 0.28$ dB/100 m is the attenuation and scattering of the radio wave in ice.

The results of measurements at typical polythermal glaciers are presented in Table 1. Table 1 shows that in the polythermal parts of glaciers, the aver-

age RPR from bedrock is 83.9–100.7 dB (on average 88.9 dB), and the difference between reflections from bedrock and CTS ranges from 5.5 to 14.2 dB (on average 8.9 dB). The values for RPR from bedrock are higher than the RPR from CTS, which ranges from 72.2 to 86.5 dB (on average 80.0 dB). The RPR from crevasses or glacier moulines decreases from 73.3 to 69.4 dB (by 3.9 dB) for the upper and middle parts of the temperate ice layer.

Radio wave velocity in cold and temperate ice

RWV in cold and temperate ice v_d and v_s were estimated using hyperbolic reflections of symmetric form (Macheret 2000). The values obtained are: $v_d = 172 \pm 0.5$ m/mcs and $v_s = 154 \pm 0.8$ m/mcs. These values can be used to determine the relative dielectric permittivity ϵ'_d and ϵ'_s of cold ice and temperate ice:

$$\epsilon'_d = (c/v_d)^2 \text{ and } \epsilon'_s = (c/v_s)^2 \quad (2)$$

and to estimate the porosity ϕ of cold ice and water content W of temperate ice using Looyenga's (1965) equations:

$$\epsilon'_d = [v_i (\epsilon'_i)^{1/3} - 1] + 1]^{1/3} \quad (3)$$

$$W = (\epsilon'_s)^{1/3} - \epsilon'_i)^{1/3} / (\epsilon'_w)^{1/3} - \epsilon'_i)^{1/3}, \quad (4)$$

where $v_i = \rho_d / \rho_i$, ρ_d is the density of cold snow, firn or glacier ice; ρ_i is the density of solid ice with density 917 kg/m³; $\epsilon'_i = 3.19 \pm 0.04$ is its relative dielectric permittivity at 0°C (Frolov and Macheret 1999); $c = 300$ m/mcs is RWV in air; $\epsilon'_w = 87.9$ is the relative dielectric permittivity of water at 0°C (Enders et al. 2009); and $\phi = 1 - v_i$. These estimates yielded the dielectric permittivity of cold and temperate ice $\epsilon'_d = 3.04$ and $\epsilon'_s = 3.79$, porosity of cold ice $\phi = 5\%$, and water content in temperate ice $W = 2.9 \pm 0.4\%$.

Thickness and volume of glaciers and cold and temperate ice

The total thickness of glaciers H_z and thickness of cold ice H_{cold} and temperate ice H_{temp} were determined by delay time τ_b of reflections from bedrock

Table 1. Average relative power of reflections (RPR) from the bedrock, CTS and buried crevasses and/or glacier moulines in temperate glaciers

Glacier name	Average RPR, dB from			Difference between average RPR of reflections from bedrock and CTS, dB
	bedrock	CTS	buried crevasses and/or glacier moulines ^{a)}	
Vestre Grønfyordbreen Upper part ^{b)}	83.9	75.3		8.6
Vestre Grønfyordbreen Lower part ^{b)}	82.7	77.2		5.5
Tungebreen	92.0	84.1		7.9
Austre Grønfyordbreen	85.4	72.2		8.2
Fridtjovbreen ^{b)}	100.7	86.5	73.3 ^{c)} 69.4 ^{d)}	14.2
Mean	88.9	80.0		8.9

^{a)} RPR of vertical series of hyperbolic reflections (VSHR) from ^{c)} 20 m and ^{d)} 60 m depth. ^{b)} Location of radar profiles is shown in Figure 1

and delay time τ_R of reflections from CTS by the upper envelope of hyperbolic reflections from water inclusions in temperate ice. Taking into account the distance d between the centres of the transmitting and receiving antennas, the thicknesses H_Σ and H_{cold} are calculated as:

$$H_\Sigma = [(\tau_B/2)^2 - (d/v_{av})^2]^{1/2} \tag{5}$$

$$H_{cold} = [(\tau_R/2)^2 - (d/v_{cold})^2]^{1/2} \tag{6}$$

and the thickness of temperate ice H_{temp} as difference between total ice thickness and thickness of cold ice as:

$$H_{temp} = H_\Sigma - H_{cold} \tag{7}$$

where v_{av} and v_{cold} is the average RWV in the whole glacier sequence and in cold ice.

For calculations, we assumed that v_{av} and v_{cold} are the same and equal to 168 m/mcs. In polythermal glaciers, v_{av} depends mainly on the ratio of thicknesses of cold and temperate ice, velocities v_{cold} and v_{temp} in cold and temperate ice and water content W in temperate ice, and can be changed from 166 to 170 m/mcs depending on the geographical location of a glacier, its thermal regime (cold or temperate), and also the distribution and thickness of snow and firn (Navarro et al. 2016). By our estimate using a two-layered model with $v_{cold}=168$ m/mcs, the average RWV in relation to a ratio of H_{cold} to H_Σ from 0 to 1 can be changed in a range from 156 to 168 m/

mcs. If we take our values 154 and 172 m/mcs derived from hyperbola reflections as references for temperate and cold ice, the errors in ice thickness estimations are +9.1% and -2.3%, respectively.

Regarding mapping the total ice thickness H_Σ , we used the RES data and points at glacier outlines where ice thickness $H_o=0$ (Lavrentiev et al. 2019). For mapping the cold ice thickness H_{cold} and temperate ice thickness H_{temp} , we also took into account the points where thickness of cold ice was $H_{cold}=0$ and ice thickness of temperate ice $H_{temp}=0$. Finally, the maps of cold and temperate ice were plotted using ArcGIS software and the Topo to Raster tool for all studied glaciers (Fig. 3).

Taking into account the possible errors of identification and selection of reflections from bedrock and CTS, the errors in measurements of delay time of τ_B and τ_R of these reflections, and values of RWV used for calculations of thickness of cold and temperate ice, we estimated the accuracy of maps by comparing measured and interpolated thickness H_Σ and H_{cold} in cross points of radar profiles. Differences in these points did not exceed ± 5 m.

Measurement data for glacier area, total ice thickness, average thickness, and volume of cold and temperate ice are presented in Table 2. The table also shows the proportion estimates of temperate ice in total volume of glaciers and of water storage in temperate ice in polythermal glaciers us-

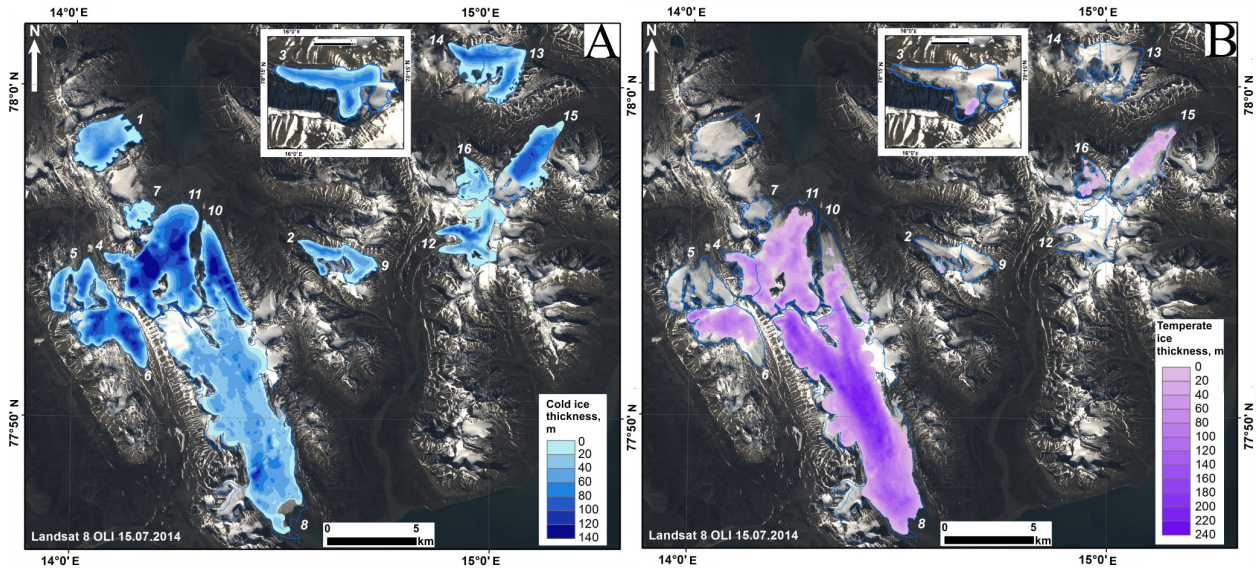


Fig. 3. Thickness of cold ice (A) and temperate ice (B) at NL glaciers according to ground-based radar measurement data in springs 1999, 2007 and 2010–2013; names of numbered glaciers are given in caption to Figure 1, and glacier margins are shown for the year of radar measurements

ing the available measurement data of RWV in temperate ice.

Errors in estimations of H_{avcold} , H_{avtemp} , V_{cold} , and V_{temp} are discussed in more detail in Section 3.

The ratio $FTIV = V_{temp} / V_{\Sigma}$ for polythermal glaciers ranges from 0.39 to 0.54 and rises to 0.73 at Fridtjovbreen. This can most likely be explained by its strong crevassing, its recent surge accompanied by penetration of water in melting periods from glacier surface into glacier sequence, and its warming.

Discussion

Errors in measurements and estimates

Detailed analysis of errors in determination of area S of glaciers in the year of RES measurements, mean H_{mean} and maximum H_{max} ice thickness, and total volume V_{Σ} of glaciers is given by Martin-Español et al. (2013, 2016), Navarro et al. (2016), Lapazaran et al. (2016a, b) and Lavrentiev et al. (2019). Below, we consider the errors in determination of other parameters of glaciers presented in Table 2, namely: average thickness of cold ice H_{avcold} and temperate ice H_{avtemp} and volume of cold ice V_{cold} and temperate ice V_{temp} .

According to previous estimations (Lavrentiev et al. 2019), the error in glacier surface S is from 2–5% to 4.53–8%; in mean ice thickness H_{mean} and maximum ice thickness H_{max} it is respectively $\pm(3-10)$ m (on average 9.9%) and $\pm(3-25)$ m (on average 8.2%); and in total volume V_{Σ} of glaciers it is $\pm 0.09-0.5$ km³, which depends on glacier area (see Table 2).

The error in determination of total ice thickness ϵ_{Hi} at i -points by data of ground penetrating radar (GPR) measurements can be estimated as per Lapazaran et al. (2016a):

$$\epsilon_{Hi} = (\epsilon_{HGPRi}^2 + \epsilon_{Hxyi}^2)^{1/2} \tag{8}$$

where ϵ_{HGPRi} and ϵ_{Hxyi} are errors of GPR and GPS measurements in i -points. The errors due to the difference in time of these measurements are small and do not exceed 0.56–1.11 m (Lapazaran et al. 2016a). The error in RES measurements of total ice thickness H_{Σ} can be estimated from the relationship (Lapazaran et al. 2016a):

$$\epsilon_{H\Sigma} = 0.5 [(\tau_B^2 \epsilon_{vav}^2 + v_{av}^2 \epsilon_{\tau B}^2)]^{1/2}, \tag{9}$$

where τ_B is the delay time of reflections from bedrock and ϵ_{vav} is the error in determination of average RWV in all glacier sequences.

Table 2. Area S of glaciers in the year of RES measurements, mean thickness of glacier H_{mean} , average thickness of cold ice H_{avcold} and temperate ice H_{avtemp} , volume of cold ice V_{cold} and temperate ice V_{temp} , measured total volume of glaciers V_{Σ} , volume fraction of temperate ice in total volume of glacier $FTIV=V_{temp}/V_{\Sigma}$, and water storage $W_s=W \times V_{temp}$ in temperate ice with water content W

Glacier	S km ²	H _{mean} ^{b)} m	H _{avcold} m	H _{avtemp} m	V _{cold} km ³	V _{temp} km ³	V _Σ ^{b)} km ³	FTIV %	W _s ^{c)} 10 ³ m ³
Baalsrubbreen	2.61 ±0.17	33±3	30±3	15±2	0.089 ±0.007	0.0009 ±0.0001	0.090 ±0.009	1.2	18
Blekumbreen	2.10 ±0.16	32±4	31±3	27±3	0.066 ±0.006	0.003 ±0.0003	0.069 ±0.007	4.0	60
Austre Dahlfonna	2.84 ±0.17	53±5	34±7	39±4	0.141 ±0.001	0.054 ±0.005	0.195 ±0.019	35.6	1,080
Vestre Dahlfonna	6.23 ±0.34	32±5	31±5	19±2	0.196 ±0.002	0.002 ±0.0002	0.198 ±0.02	1.0	42
Erdmannbreen	8.14 ±0.24	92±9	62±6	49±4	0.504 ±0.05	0.249 ±0.025	0.753 ±0.075	23.1	4,980
Vestre Field ^{a)}	1.79 ±0.12	11±2	11±2	0	0.020 ±0.002	0	0.020 ±0.02	0	0
Fridtjovbreen	47.31 ±1.01	107±10	29±3	96±9	1.352 ±0.14	3.733 ±0.037	5.085 ±0.5	73.8	74,660
Gleditschfonna ^{a)}	2.26 ±0.12	26±3	26±2	0	0.059 ±0.006	0	0.059 ±0.06	0	0
Austre Grøn-fjordbreen	7.59 ±0.27	61±8	61±6	39±4	0.466 ±0.005	0.104 ±0.001	0.570 ±0.057	17.1	2,080
Vestre Grøn-fjordbreen	17.58 ±0.43	66±9	66±6	37±4	1.131 ±0.12	0.486 ±0.047	1.617 ±0.161	24.1	9,720
Marstrander-breen ^{a)}	6.24 ±0.32	29±4	29±3	6±2	0.179 ±0.018	0.001 ±0.0001	0.180 ±0.018	0.6	20
Austre Passfjellbreen ^{a)}	5.46 ±0.29	33±4	33	0	0.181 ±0.018	0	0.181 ±0.018	0	0
Vestre Passfjellbreen	2.51 ±0.14	37±5	37	0	0.090 ±0.009	0	0.09 ±0.09	0	0
Tavlebreen	7.47 ±0.30	51±5	51	10±1	0.370 ±0.03	0.030 ±0.003	0.400 ±0.04	15.8	608
Tungebreen	2.91 ±0.18	22±3	22	21±2	0.059 ±0.06	0.010 ±0.001	0.069 ±0.007	10.8	200
Total	123.04 ±0.36				4.903 ±0.45	4.673 ± 0.5	9.576 ±0.34		93,468 ± 1,700

^{a)} Glaciers consisting of cold ice; ^{b)} Data for area S, mean ice thickness H_{mean} , total volume V_{Σ} of glaciers and errors in their estimates are given by Lavrentiev et al. (2019); ^{c)} Values of water storage W_s in polythermal glaciers are given for estimated average water content W in temperate ice 2%

At maximum total ice thickness of glaciers, $H_{\Sigma}=280$ m, $v_{av}=168$ m/mcs, and $\epsilon_{vav}=\pm(1.7-8.45)$ m/mcs and $\epsilon_{\tau B}=\pm 0.05$ mcs (Lapazaran et al. 2016a), the $\epsilon_{H_{\Sigma}}$ will be $\pm(7-16)$ m $\pm(2.5-5.7\%)$ and will linearly depend on H_{Σ} .

Errors in determination of cold ice thickness H_{cold} and temperate ice H_{temp} can be estimated using the similar relationships:

$$\epsilon_{H_{cold}} = 0.5 [\tau_R^2 \epsilon_{vcold}^2 + v_{cold}^2 \epsilon_{\tau R}^2]^{1/2} \tag{10}$$

$$\epsilon_{H_{temp}} = 0.5 [(\tau_B - \tau_R)^2 \epsilon_{vtemp}^2 + v_{temp}^2 \epsilon_{\tau R}^2]^{1/2}, \tag{11}$$

where τ_R is the delay time of reflections from CTS, v_{emp} is RWV in temperate ice, ϵ_{vtemp} is the error in its determination.

At maximum ice thickness of cold ice $H_{cold}=140$ m, $v_{cold}=168$ m/mcs, $\epsilon_{vcold}=\pm 2$ m/mcs, $\epsilon_{\tau R}=\pm 0.05$ mcs, $\epsilon_{H_{cold}}=\pm 6.4$ m ($\pm 4.6\%$).

In polythermal glaciers, the RWV in temperate ice v_{temp} can range from 156 to 168 m/mcs; i.e., on average $v_{temp} = 162$ m/mcs, $\epsilon_{vtemp} = \pm 6$ m/mcs and depends on water content W in temperate ice. At maximum thickness of temperate ice $H_{temp} = 240$ m, $\epsilon_{Htemp} = \pm 5.7$ m ($\pm 2.4\%$).

Common uncertainties for ice thickness measurements arise from errors in determination of RWV in glacier sequence and inaccuracy in selection of delay time of radar reflections, and they depend on the distance between the RES profile and measurement points and glacier outlines. This leads to interpolation errors ϵ_{Hintk} at the construction of ice-thickness digital elevation models (DEMs) and maps using different automatic interpolation algorithms (Topo to Raster, kriging, inverse distance weighting, or spline).

The contribution of errors ϵ_{Hintk} at regular k-points of interpolation grid to ice thickness H_k measurements and can be estimated as per Lapazaran et al. (2016b):

$$\epsilon_{Hk} = (\epsilon_{Hdatai}^2 + \epsilon_{Hintk}^2)^{1/2} \tag{12}$$

This relationship can be used to estimate the errors in construction of total ice thickness and cold and temperate ice thickness maps.

Interpolation errors ϵ_{Hintk} using kriging interpolation methods were considered by Lapazaran et al. (2016b) and Krivoruchko (2012) and were estimated on the example of Werenskioldbreen in Svalbard (Lapazaran et al. 2016b) and two sites at the Guliya ice cap in Tibet (Guliya Summit and Guliya Plateau) (Kutuzov et al. 2016). It was found that the interpolation error ϵ_{Hintk} depends on average ice thickness H_{av} . For Werenskioldbreen, with H_{av} of 107.65 m, the mean interpolation mean error ϵ_{Hintk} was estimated as 4.41 m (4.1%); for Guliya Summit with H_{av} of 228.76±11.69 m – as 18.38 m (8%); and for Guliya Plateau with H_{av} of 42.55 m – as 2.4 m (5.6%).

Greater interpolation errors ϵ_{Hintk} were obtained using the Topo to Raster method with RES data measurements at 16 glaciers and ice caps in Norway within an interpolated area ranging from 0.2 to 310 km², average ice thickness ranging from 6 to 183 m, and uncertainty in interpolated volume (15–20%) σ from ±0.1 to ±9.3 km³ (Andreassen et al. 2015). According to these data, the mean estimated error in interpolated ice thickness at each grid

point was 15–20% and the best accuracy (15%) is expected for glaciers with more dense spatial coverage by RES data.

To estimate the errors for construction of cold and temperate ice thickness maps of glaciers in NL, we also used the Topo to Raster method, but calculated the sum of the measured average thicknesses of cold ice H_{avcold} and temperate ice divided by the number of corresponding points only in the bound of radar profiles with measured thicknesses of cold ice H_{cold} and temperate ice H_{temp} ; i.e., not considering the parts of glaciers between points on radar profiles and points with ice thickness $H_0=0$ and points with cold ice thickness $H_{cold}=0$ and temperate ice thickness $H_{temp}=0$. The difference between interpolated and measured values H_{avcold} and H_{avtemp} does not exceed 10%, which is between three quarters and half the previous estimates for the 16 glaciers in Norway and better agrees with our above-mentioned estimations.

The total volume of glaciers V_{Σ} was determined using DEMs of total ice thickness H_{Σ} as sum of product of area of cells A_k by total ice thickness $H_{\Sigma k}$ in each cell of the interpolation grid (Martin-Español et al. 2016; Lavrentiev et al. 2019):

$$V_{\Sigma} = \Sigma A_k H_k. \tag{13}$$

The same approach was used to estimate the volume of cold and temperate ice.

Considering the errors $\epsilon_{H\Sigma}$ in determination of area S of glaciers, the total error $\epsilon_{V\Sigma}$ in determination of total volume of glaciers V_{Σ} can be estimated as:

$$\epsilon_{V\Sigma} = (\epsilon_S^2 + \epsilon_{H\Sigma}^2)^{1/2}. \tag{14}$$

At $\epsilon_S=4.53-8\%$ and maximum error $\epsilon_{H\Sigma}=2.5-5.7\%$, the error $\epsilon_{V\Sigma}$ will be from 5.2–7.3% to 8.4–9.8% and the error in determination of volume of temperate ice ϵ_{Vtemp} will be 5.1–8.3%.

RWV in temperate ice

According to data from CMP measurements at Fridtjovbreen in spring 1988, before its surge in the 1990s, the RWV in temperate ice v_{temp} was 167.3±4.3 m/mcs (Macheret and Glazovsky 2000),

which corresponds to water content $W=0.1\pm 1.0\%$. It differs from $v=154\pm 0.8$ m/mcs and water content $W=2.9\pm 0.4\%$ estimated by hyperbolic reflections recorded at Fridtjovbreen in spring 2012 and Austre Grønfyordbreen in spring 2010. In other polythermal glaciers, these values were estimated as 157–167 m/mcs (on average 164 ± 4.2 m/mcs) and correspond to water content in temperate ice 0.2–3.2% (on average $2.2\pm 0.9\%$) (Glazovsky and Macheret 2014) with typical values of 1–2% (Dowdeswell and Evans 2004). Keeping in mind the range of assessments and level of uncertainty, we took as representative the water content in temperate ice $W=2\%$ for estimation of water storage W_s in polythermal glaciers in NL (see Table 2).

Water at CTS and bedrock

The data presented in Table 1 show that differences in RPR from CTS and bedrock indicate the connection between intensity of radar reflections from water inclusions in temperate ice at these interfaces and can be useful for identification of their origin and estimation of relative spatial water content changes in glacier sequence and at the bottom. Repeated RPR measurements can also be useful for the study of temporally changing processes in buried crevasses, glacier moulins and englacial conduits and channels, as important elements of englacial drainage systems and pathways of entering and inflow of water to glacier bodies and bedrock in melt periods. Application of the SSAA module can be effective for this aim and allows the difference in relative dielectric permittivity of cold and temperate ice and bedrock to be estimated.

Using the above estimated values of relative dielectric permittivity of cold ice ϵ'_d and temperate ice ϵ'_s , it is possible to calculate the power reflection coefficient (PRC) $R_{1,2}$ from the flat boundary of cold and temperate ice and power reflection coefficient $R_{2,3}$ from the flat boundary of temperate ice and bedrock as:

$$R_{1,2} = 20 \lg \left(\frac{[\epsilon'_1{}^{1/2} - \epsilon'_2{}^{1/2}]}{[\epsilon'_1 + \epsilon'_2]} \right); \quad (15)$$

$$R_{2,3} = 20 \lg \left(\frac{[\epsilon'_{1,2}{}^{1/2} - \epsilon'_3{}^{1/2}]}{[\epsilon'_{1,2} + \epsilon'_3]} \right), \quad (16)$$

where indexes 1 and 2 denote, respectively, cold and temperate ice; index 3 denotes glacier bedrock.

With the above estimated values $\epsilon'_1=3.04$, $\epsilon'_2=3.79$ and assuming a value of $\epsilon'_3=5$, we obtained $R_{1,2}=-24.9$ dB and $R_{2,3}=-18.6$ dB. This means that PRC from bedrock exceeds PRC from boundary of cold and temperate ice (CTS) by 6.5 dB, which is close to estimates using the SSAA module (see Table 1).

These estimations agree with data of airborne RES measurements at a frequency of 60 MHz along longitudinal profiles of polythermal glaciers in different regions of Svalbard (Bamber 1989), where PRC from bedrock varies from -7.4 to -15.9 dB and exceeds the PRC from CTS ranging from -18.0 to -27.1 dB by 10.6–11.2 dB.

A similar pattern was observed at the polythermal glacier Olivares Alfa in the Chilean Andes by airborne RES data: the average PRC from CTS at a frequency of 50 MHz (Gacitúa et al. 2015) was about -30 dB and from bedrock about -20 dB; i.e., PRC from bedrock exceeds PRC from CTS by ~10 dB and varies from -20 to -30 dB due to variations in the dielectric permittivity of the bedrock ϵ'_3 in a range from 4 to 10.

Icings and suspended sediment plums at terminus of polythermal glaciers

RES data shows (see Table 2) that polythermal glaciers in NL contain from 0.0009 to 3.733 km³ of temperate ice and, with estimated water content of 2%, can accumulate from $18\cdot 10^3$ m³ to $74.660\cdot 10^3$ m³ of liquid water. This amount can be enough to serve as a source of englacial and subglacial run-off, feeding of water streams and near-glacier lakes and forming the near-glacier icings at the terminuses of land-terminated glaciers and the suspended sediment plums in the sea at the front of tidewaters. In NL, in springtime, we observed near-glacier icings at Austre Grønfyordbreen, Vestre Grønfyordbreen, and Fridtjovbreen. In general, near-glacier icings have been observed in many other regions of Spitsbergen (Gokhman 1987; Bukowska-Jania and Szafranec 2005). In wintertime, the englacial run-off flowed from Bertilbreen and was used to supply water to the Pyramiden mine (Zhuravlev et al. 1983). Subglacial water run-off leading to desalination of sea water was detected in winter near the ice front of Tunabreen (Muzylyev et al. 2013). Taking into account that in Svalbard there are 163 tidewa-

ter glaciers with a total ice-front length of 860 km (Błaszczyk et al. 2009), subglacial run-off can have a remarkable influence on the spread of sea ice in adjoining fjords (Marchenko et al. 2017).

Conclusions

1. Data from ground-based RES measurements performed in the springs of 1999, 2007, and 2010–2013 on 16 glaciers in Nordenskiöld Land, Svalbard, showed that five of them relate to glaciers with a cold thermal regime and 11 to glaciers with a polythermal regime. For their identification, we used the differences in character of radar reflections from the upper and lower parts of glacier sequence: absence of internal reflections (excluding reflections from buried crevasses and glacier moulins) from the upper cold ice layer and a great number of reflections of hyperbolic form from the lower layer connected with strong scattering of radio waves on water inclusions in temperate ice. It was found that the relative power of radar reflections (RPR) from CTS is smaller by 5.5–14.2 dB compared to those from bedrock, which can be considered an indicator of less water content at CTS than at bedrock. Repeated RPR measurements can be used for estimation of spatial and temporal changes in water content at these boundaries.

2. Polythermal glaciers have the upper layer of cold ice with mean ice thickness from 11 ± 2 to 66 ± 6 m and the near-bottom layer of temperate water-saturated ice with mean ice thickness from 6 ± 2 m to 96 ± 9 m. The ratio of mean thickness of cold and temperate ice varies from 0.30 to 5.31, and the volume fraction of temperate ice in total volume of glaciers with polythermal regime varies from 1% to 74%.

3. Thickness of cold ice was defined by measured delay time of radar reflections from cold-temperate surface (CTS) and thickness of temperate ice as difference between total glacier thickness and cold ice thickness.

4. It was found that in polythermal glaciers the volume of temperate ice varied from 1% to 74% of the total volume, which equalled 4.67 ± 0.4 km³ and occupied 51% of total volume in all measured polythermal glaciers. At proposed water average, water

content 2% in temperate ice in these glaciers can be stored from 18×10^3 to 74.660×10^3 m³ of liquid water. This volume may be enough to produce englacial and subglacial run-off and near-glacier icings in wintertime.

5. Vertical series of hyperbolic reflections (VSHR), connected with buried crevasses and/or glacial moulins were observed to depths reaching CTS, near-bottom temperate ice, and bedrock. They can be used to detect the possible sites and pathways of water inflow to glacier sequence and bedrock at melting periods and influence on viscosity and fluidity of ice deformation and bottom sliding of polythermal glaciers. Repeated measurements of RPR from CTS, buried crevasses, and/or glacier moulins and bedrock can also be used for the study of processes in englacial and subglacial drainage systems connected to such glaciers.

6. RES data obtained on depth of CTS and thickness of cold ice layer can be used as boundary conditions for numerical modelling and estimation of regional climate changes. This approach was applied for Grønfjordbreen, using the data on CTS depth change for a 33-year period (1979–2012), when the average thickness of the cold ice layer decreased by 34 m. Comparison of calculated and modelled cold ice thicknesses have shown (Sosnovsky et al. 2016) that such a change could have occurred in the ablation area of the glacier due to regional climate warming by 0.6°C and this estimate is close to the measured increase in annual mean air temperature at nearest weather station.

7. The large CTS variations, relatively thin cold ice and relatively thick temperate ice on Fridtjovbreen might be explained as consequences of surge, and related with development of crevasse areas with different water inflow. Thin glaciers (20–30 m on average) even with different areas (from 2 to 6 km²) reveal very small or even no temperate ice core.

Acknowledgements

This study was supported by RF State Contract 0148-2019-0004 (AAAA-A19-119022190172-5). Data processing was funded by grant 18-05-60109, and mapping by the RFBR grant 18-05-60067.

Disclosure statement

No potential conflict of interest was reported by the authors.

Author Contributions

Study design: I.L., Y.M.; data collection I.L.; statistical analysis A.G.; interpretation of results A.G., I.L., Y.M.; preparation of manuscript A.G., Y.M.; literature review: Y.M.

References

- ANDREASSEN LM, HUSS M, MELVOLDT K, ELVERHOY H and WINSWOLD SH, 2015, Ice thickness measurements and volume estimates for glaciers in Norway. *Journal of Glaciology* 61(228): 764-775, DOI: <http://doi.org/10.3189/2015Jog14J161>
- ASCHWANDEN A and BLATTER H, 2005, Meltwater production due to strain heating in Stor-glaciären. Sweden. *Journal of Geophysical Research* 110(F4): F04024.2005, DOI: <http://doi.org/10.1029/2005JF000328>
- ASCHWANDEN A, BUELER E, KHROULEV C and BLATTER H, 2012, An enthalpy formulation for glaciers and ice sheets. *Journal of Glaciology* 58(209): 441-457, DOI: <http://doi.org/10.3189/2012Jog11J088>
- BÆLUM K and BENN D, 2011, Thermal structure and drainage system of a small valley glacier (Tellbreen, Svalbard), investigated by ground penetrating radar. *The Cryosphere* 5: 139-149, DOI: <http://doi.org/10.5194/tc-5-139-2011>
- BAMBER JL, 1987, Internal reflecting horizons in Spitsbergen glaciers. *Annals of Glaciology* 9: 5-10.
- BAMBER JL, 1988, Enhanced radar scattering from water inclusions in ice. *Journal of Glaciology* 34(118): 293-296.
- BAMBER JL, 1989, Ice/bed interface and englacial properties of Svalbard ice masses from airborne radio-echo sounding. *Journal of Glaciology* 35(119): 30-37.
- BARRETT BE, MURRAY T and CLARK R, 2007, Errors in radar CMP velocity estimates due to survey geometry and their implication for ice water content estimation. *Journal of Environmental and Engineering Geophysics* 12(1): 101-111.
- BJÖRNSSON H, GJESSING Y, HAMRAN S-E, HAGEN JO, LIESTØL O, PÁLSSON F and ERLINGSSON B, 1996, The thermal regime of sub-polar glaciers mapped by multi-frequency radio-echo sounding. *Journal of Glaciology* 42(140): 23-32.
- BŁASZCZYK M, JANIA JA, HAGEN JO, 2009, Tidewater glaciers of Svalbard: Recent changes and estimates of calving fluxes. *Polish Polar Research* 30(2): 85-142.
- BLATTER H and GREVE R, 2015, Comparison and verification of enthalpy schemes for polythermal glaciers and ice sheets with a one-dimensional model. *Polar Science* 9: 197-207.
- BUKOWSKA-JANIA E, SZAFRANIEC J, 2005, Distribution and morphometric characteristics of icing fields in Svalbard. *Polar Research* 24 (1-2): 41-53.
- DOWDESWELL JA, DREWRY DJ, LIESTØL O and ORHEIM O, 1984, Airborne radio echo sounding of sub-polar glaciers in Spitsbergen. *Norsk Polarinstituttet Skrifter* 182: 1-42.
- DOWDESWELL JA and EVANS S, 2004, Investigations of the form and flow of ice sheets and glaciers using radio-echo sounding. *Reports on Progress in Physics* 67(10): 1821-1861
- DUVAL P, 1977, The role of water content on the creep of polycrystalline ice. *IAHS Publication* 118: 29-33.
- ENDRES AL, MURRAY T, BOOTH AD and WEST LJA, 2009, A new framework for estimating englacial water content and pore geometry using combined radar and seismic wave velocities. *Geophysical Research Letters* 36(4): L04501, DOI: <http://doi.org/10.1029/2008GL036876>
- FROLOV AD and MACHERET YY, 1999, On dielectric properties of dry and wet snow. *Hydrological Processes* 13: 1755-1760.
- GACITÚA G, URBINE J A, WILSON R, LORIAUX T, HERNANDEZ J and RIVERA A, 2015, 50MHz helicopter-borne radar data for determination of glacier thermal regime in the central Chilean Andes. *Annals of Glaciology* 56(70): 93-101, DOI: <http://doi.org/10.3189/2015AoG70A953>
- GLAZOVSKY AF, KRASS MS and MACHERET YY, 1988, Peculiarities in dynamics of subpolar glaciers under climate changes. *Data of Glaciological Studies* 85: 187-195.
- GLAZOVSKY AF and MACHERET YY, 2014, *Water in glaciers. Results of geophysical and remote sensing studies*. GEOS, Moscow.

- GOKHMAN VV, 1987, Spreading and formation conditions of icings in Spitsbergen. *Data of glaciological studies* 89: 68-76.
- GRABIEC M, JANIA J, PUCZKO D, KOLONDRÁ L, BUDZIK T, 2012, Surface and bed morphology of Hansbreen, a tidewater glacier in Spitsbergen. *Polish Polar Research* 33(2): 111-138. DOI: <http://doi.org/10.2478/v10183-012-0010-7>
- HEWITT I J and SCHOOF C, 2017, Models for polythermal ice sheets and glaciers. *The Cryosphere* 11: 541-551, DOI: <http://doi.org/10.5194/tc-11-541-2017>
- JANIA J, MACHERET YY, NAVARRO FJ, GLAZOVSKY AF, VASILENKO EV, LAPAZARAN J, GLOWACKI P, MIGALA K, BALUT A and PIWOWAR BA, 2005, Temporal changes in the radiophysical properties of a polythermal glacier. *Annals of Glaciology* 42: 125-134.
- JISCOOT H, MURRAY T and BOYLE P, 2000, Controls on distribution of surge-type glaciers. *Journal of Glaciology* 46(154): 411-422.
- KRIVORUCHKO K, 2012, Empirical Bayesian Kriging implemented in ArcGIS Geostatistical Analyst. *ArcUser* 15(4): 6-10.
- KULNITSKY LM, GOFMAN PA and TOKAREV MY, 2001, Mathematical processing of georadar data and RADEXPRO system, *Razvedka. Okhrana nedr* 3: 6-11.
- KUTUZOV S, THOMPSON LG, LAVRENTIEV I and TIAN L, 2018, Ice thickness measurements of Guliya ice cap, western Kunlun Mountains (Tibetan Plateau), China. *Journal of Glaciology* 64(248): 977-989, DOI: <http://doi.org/10.1017/jog.2018.91>
- LAPAZARAN JJ, OTERO J, MARTIN-ESPAÑOL A and NAVARRO FJ, 2016a, On the errors involved in ice-thickness estimates I: ground-penetrating radar measurement errors. *Journal of Glaciology* 62(236): 1008-1020, DOI: <http://doi.org/10.1017/jog.2016.93>
- LAPAZARAN JJ, OTERO J, MARTIN-ESPAÑOL A and NAVARRO FJ, 2016b, On the errors involved in ice-thickness estimates II: errors in digital elevation models of ice thickness. *Journal of Glaciology* 62(236): 1021-1029, DOI: <http://doi.org/10.1017/jog.2016.94>
- LAVRENTIEV II, GLAZOVSKY AF, MACHERET YY, MURAVYEV AY and MATSKOVSKY VV, 2019, Reserves of ice in glaciers on the Nordenskiöld Land, Spitsbergen and their changes over the last decades. *Ice and Snow* 59(1): 23-38.
- LOOYENGA H, 1965, Dielectric constants of heterogeneous mixture. *Physica* 31(3): 401-406.
- MACHERET YY, 2000, Estimation of water content in glaciers using hyperbolic reflections. *Data of glaciological studies* 89: 3-10.
- MACHERET YY, BERIKASHVILI VS, VASILENKO EV, SOKOLOV VG, 2006, Broadband pulse radar for sounding glaciers with optical synchronization channel and digital signal processing. *Sensors and Systems* 12, 2-8.
- MACHERET YY and GLAZOVSKY AF, 2000, Estimation of absolute water content in Spitsbergen glaciers from radar sounding data. *Polar Research* 19(2): 205-216.
- MACHERET YY and ZHURAVLEV AB, 1982, Radio-echo sounding of Svalbard glaciers. *Journal of Glaciology* 28(99): 295-314.
- MARCHENKO AV, MOROZOV EG and MARCHENKO AN, 2017, Supercooling of seawater near the glacier front in a fjord. *Earth Science Research* 6(1): 97-108.
- MARTIN-ESPAÑOL A, VASILENKO EV, NAVARRO FJ, OTERO J, LAPAZARAN JJ, LAVRENTIEV II, MACHERET YY and MACHIO F, 2013, Radio-echo sounding and ice volume estimates on western Nordenskiöld Land, Svalbard. *Annals of Glaciology* 54(64): 211-217, DOI: <http://doi.org/10.3289/2013AoG64A109>
- MARTIN-ESPAÑOL A, LAPAZARAN JJ, OTERO J and NAVARRO FJ, 2016, On the errors involved in ice-thickness estimates III: error in volume. *Journal of Glaciology* 62(236):1030-1036, DOI: <http://doi.org/10.1017/jog.2016.95>
- MURRAY T, JAMES TD, MACHERET YY, LAVRENTIEV II, GLAZOVSKY AF and SYKES H, 2012, Geometric changes in a tidewater glacier in Svalbard. *Arctic, Antarctic, and Alpine Research* 44(3): 359-367.
- MURRAY T and PORTER PR, 2001, Basal conditions beneath a soft-bedded polythermal surge-type glacier: Bakaninbreen, Svalbard. *Quaternary International* 86(1): 103-116. DOI: [http://doi.org/10.1016/S1040-6182\(01\)00053-2](http://doi.org/10.1016/S1040-6182(01)00053-2)
- MUZYLEV SV, MACHERET YY, MOROZOV EG, LAVRENTIEV II, MARCHENKO AV, 2013, Fluctuations of ice cover and sea water pressure nearby the Tunabreen Glacier front at Spitsbergen. *Ice and Snow* 53(4): 119-124 DOI: <http://doi.org/10.15356/2076-6734-2013-4-119-124>
- NAVARRO FJ, GLAZOVSKY AF, VASILENKO EV, CORCUERA MI and CUADRADO L, 2005, Ice volume changes (1936-1990) and structure of Aldegondabreen. Spitsbergen. *Annals of Glaciology* 42: 158-162.

- NAVARRO FJ, LAPAZARAN JJ, MARTIN-ESPAÑOL A and OTERO J, 2016, Ground-penetrating radar studies in Svalbard aimed to the calculation of the ice volume of its glaciers. *Cuadernos de Investigacion Geografica* 42(1): 399-414, DOI: <http://doi.org/10.18172/cig.2929>
- ØDEGAARD RS, O., HAFEN JO and HAMRAN S-E, 1997, Comparison of radio-echo sounding (30-1000 MHz) and high-resolution borehole-temperature measurements at Finsterwalderbreen, southern Spitsbergen, Svalbard. *Annals of Glaciology* 24: 262-267.
- PFEFFER WT, ARENDT AA, BLISS A, BOLCH T, COGLEY JG, GARDNER AS, HAGEN JO, HOCK R, KASER G, KIENHOLZ C, MILES ES, MOHOLDT G, MÖLG N, PAUL F, RADIC' V, RASTNER P, RAUP BH, RICH J, SHARP MJ, THE RANDOLPH CONSORTIUM, 2014, The Randolph Glacier Inventory: A globally complete inventory of glaciers. *Journal of Glaciology* 60(221): 537-552. DOI: <http://doi.org/10.3189/2014JoG13J176>
- RGI CONSORTIUM. 2017. *Randolph Glacier Inventory – A Dataset of Global Glacier Outlines: Version 6.0: Technical Report. Global Land Ice Measurements from Space*. Colorado. USA. Digital Media. DOI: <http://doi.org/10.7265/N5-RGI-60>
- SEVESTRE H, BENN DI, J. HULTON NR and BÆLUM K, 2015, Thermal structure of Svalbard glaciers and implications for thermal switch models of glacier surging. *Journal of Geophysical Research: Earth Surface* 120(10): 2220-2236, DOI: <http://doi.org/10.1002/2015JF003517>
- SOSNOVSKY AV, MACHERET YY, GLAZOVSKY AF and LAVRENTIEV II, 2016, Hydrothermal structure of a polythermal glacier in Spitsbergen by measurements and numerical modeling. *Ice and Snow* 56(2): 149-160.
- VASILENKO EV, GLAZOVSKY AF, LAVRENTIEV II and MACHERET YY, 2014, Changes of hydrothermal structure of Austre Grøn fjordbreen and Fridtjovbreen in Spitsbergen. *Ice and Snow* 1(125): 5-19.
- VASILENKO E, MACHIO F, LAPAZARAN J, NAVARRO FJ and FROLOVSKIY K, 2011, A compact lightweight multipurpose ground-penetrating radar for glaciological applications. *Journal of Glaciology* 57(206): 1113-1118. Doi: <http://doi.org/10.3189/002214311798843430>
- ZHURAVLEV AB, BOBROVA LI and MACHERET YY, 1993, Radio-echo-sounding of a polar glacier with summer water run-off. *Data of glaciological studies* 46: 143-149.

Received 16 August 2019
Accepted 21 December 2019